Available online at www.sciencedirect.com
ScienceDirect
European Journal of Pharmaceutics and Biopharmaceutics 65 (2007) 68–77
European Journal of Pharmaceutics and Biopharmaceutics
www.elsevier.com/locate/ejpb

Research paper

Nanoparticles based on *N*-trimethylchitosan: Evaluation of absorption properties using in vitro (Caco-2 cells) and ex vivo (excised rat jejunum) models

Giuseppina Sandri [a], Maria Cristina Bonferoni [a], Silvia Rossi [a], Franca Ferrari [a], Sara Gibin [a], Ylenia Zambito [b], Giacomo Di Colo [b], Carla Caramella [a,*]

[a] *Department of Pharmaceutical Chemistry, University of Pavia, Pavia, Italy*
[b] *Department of Bioorganic Chemistry and Biopharmaceutics, University of Pisa, Pisa, Italy*

Received 31 January 2006; accepted in revised form 13 July 2006
Available online 27 July 2006

Abstract

Among the chitosan derivatives, trimethylchitosan (TMC) has been shown to have penetration enhancement properties also in intestinal environment. In addition, the use of nanoparticulate systems has the advantage of protecting peptidic drugs from intestinal degradations, due to internalisation behaviour. Therefore, the aim of this paper was to evaluate nanoparticulate systems based on TMC. In particular the mucoadhesive and absorption enhancement properties of nanoparticles based on TMC with different quaternization degree (QD) intended for the intestinal administration of macromolecules (peptides) have been evaluated. Comparison with chitosan (CS·HCl) nanoparticles was made. The nanoparticles were loaded with fluorescein isothiocyanate dextran (FD4, MW 4400 Da), used as the model macromolecule. The intestinal penetration enhancement properties of nanoparticles were investigated in an in vitro Caco-2 cell model and an ex vivo rat jejunum model. The mucoadhesion of the nanosystems was evaluated using excised rat jejunum. All of the nanoparticulate systems interacted with the Caco-2 cells decreasing the transepithelial electric resistance (TEER) and increasing Lucifer Yellow (LY) Papp (paracellular pathway marker). All the nanosystems improved FD4 Papp, with the exception of the nanoparticles based on TMC with the highest QD. In this case an entrapment of nanoparticles into Caco-2 cells was supposed. Analogous results were obtained using the excised rat jejunum model. The increase in QD of TMC was seen to favour the mucoadhesion, resulting in a prolonged residence time on intestinal mucosa. The nanoparticle penetration into excised rat jejunum tissue, observed by means of CLSM, suggested that the mucoadhesive properties delayed the absorption of nanoparticles, however they produced an increase in the contact time with intestinal epithelium, offering a better chance for internalisation. The improvement of mucoadhesion and of nanoparticle internalisation with respect to chitosan nanosystems makes the TMCs nanosystems suitable carriers for the intestinal absorption of peptides.

Keywords: Trimethylchitosan nanoparticles; Absorption properties; In vitro Caco-2 cell model; Ex vivo rat jejunum model; CLSM

1. Introduction

Significant advances in biotechnology and biochemistry have led to the discovery of a large number of bioactive molecules and vaccines based on peptides and proteins. The parenteral route, invasive and characterized by poor patient compliance, still remains the most employed. Moreover such macromolecules are unstable and characterized by short half-life, so frequent injections are required.

The poor bioavailability of peptide drugs when administered via oral route depends on the rapid hydrolytic and enzymatic degradation in contact with the gastrointestinal fluids and is also a consequence of poor absorption through the GI epithelium.

* Corresponding author. Department of Pharmaceutical Chemistry, School of Pharmacy, University of Pavia, V.le Taramelli, 12, 27100 Pavia, Italy. Tel.: +39 0382 987385; fax: +39 0382 422975.
E-mail address: carla.caramella@unipv.it (C. Caramella).

0939-6411/$ - see front matter © 2006 Elsevier B.V. All rights reserved.
doi:10.1016/j.ejpb.2006.07.016

Recently, nanoparticulate systems have been identified as suitable peptide/protein carriers. In particular nanoparticles are able to protect drugs from degradation, to improve permeation/penetration of the drugs across mucosal surface and also to control the release of the encapsulated or adsorbed drug [1–3].

Nanoparticles possess marked mucoadhesion properties that have been related to the combination of the particle size and the particle superficial charge [4]. Furthermore nanoparticles have been referred to as capable of being absorbed into mucosal tissue [5].

Chitosan is a cationic polysaccharide characterized by good mucoadhesive properties [6,7], and has been shown to be a penetration enhancer in acidic environment towards monostratified and pluristratified epithelia both endowed with and lacking tight junctions [8,9].

Chitosan nanoparticles are able to be internalised into intestinal, nasal and ocular epithelial cells [10–13]. The uptake of chitosan nanoparticles seems to be related to the size and the superficial charge: the higher the superficial positive charge, the stronger is the affinity between nanoparticles and the negatively charged cell membranes [14,15].

N-Trimethylchitosan chloride (TMC), a chitosan derivative synthesized by the partial quaternization (trimethylation) of chitosan, is characterized by fixed positive charges irrespective of pH [16–18]. TMC has proved as an effective penetration enhancer of hydrophilic and/or high molecular weight molecules across the intestinal epithelium [16–20] even in neutral environments by means of the same mechanism of chitosan (tight junctions opening and widening of paracellular pathway). The TMC charge density, determined by the quaternization degree, is a key factor in obtaining both the mucoadhesion [20] and the penetration enhancement towards intestinal [16–19,21] epithelium. Until now, to our knowledge, no evaluation of TMC nanoparticulate systems designed for intestinal delivery has been performed.

Given these premises, the aim of the present work was to develop nanoparticulate systems based on trimethylchitosan and intended for the intestinal transmucosal administration of high molecular weight hydrophilic molecules, such as peptides. The nanosystems were loaded with a model macromolecule, fluorescein isothiocyanate dextran (MW 4400 Da). Three trimethylchitosans, with different quaternization (trimethylation) degrees, synthesized from the same chitosan (580 kDa), were selected. The nanoparticles obtained with the starting chitosan and the derived trimethylchitosan were prepared by means of ionotropic gelation [23].

The penetration enhancement properties of nanoparticles were investigated using two different approaches: in vitro permeation test on Caco-2 cell monolayers and ex vivo study using excised rat jejunum.

All the nanoparticulate systems were characterized for mucoadhesion properties towards excised rat jejunum by means of "washability" tests simulating the in vivo removal effects of intestinal fluids exerted by the peristalsis and by the gastrointestinal content.

Both the Caco-2 cell monolayers and the intestinal tissue were subjected, after treatment, to microscopic analysis by means of Confocal Laser Scanning Microscopy (CLSM) to identify the pattern of interaction of the nanoparticles with the biological substrates, in particular their internalization behaviour.

2. Materials and methods

2.1. Materials

The trimethylchitosans were obtained from a chitosan 90% deacetylated (MW 580 kDa), from shrimp (CS·HCl) (Chito-clear FG90, Primex, N) using procedures described in the literature [22,23]. A series of three trimethylchitosan hydrochloride, which differed in quaternization degree (QD), was obtained: TMC1 (QD = 4%), TMC2 (QD = 35%), TMC3 (QD = 90%). All the polymers were previously characterized by Di Colo et al. [25]. Pentasodium tripolyposphate (TPP) (Sigma, I) was used as chitosan and trimethylchitosan cross-linking agent.

Fluorescein isothiocyanate dextran (FD4) (Sigma, I), a hydrophilic and high MW molecule (MW 4400 Da), was used as a model.

Lucifer Yellow (LY) (Sigma, I) was used as a hydrophilic marker of the tight junction integrity (paracellular pathway).

2.2. Methods

2.2.1. Nanoparticle preparation

Chitosan and trimethylchitosan nanoparticles were prepared according to the mild procedure previously developed by Calvo et al. [24] based on ionotropic gelation of chitosan and trimethylchitosans (polycations) with TPP polyanion. The ionotropic gelation takes place when the positively charged amino groups of chitosan and trimethylchitosans interact with the negatively charged TPP. Chitosan and trimethylchitosans were dissolved at 2.5 mg/ml in distilled water by means of gentle stirring while TPP was dissolved at 1.25 mg/ml in distilled water. The optimal weight ratio between polymer and TPP was evaluated by means of turbidimetric analysis [25]. Different amounts of TPP solution were added by drops to 3 ml of chitosan or trimethylchitosan solutions and the mixture was diluted to 4.5 ml. Therefore the mixtures based on polymers and TPP were prepared with a fixed chitosan concentration of 1.67 mg/ml and TPP concentrations ranging from 0.07 to 0.42 mg/ml. The turbidity of each mixture was evaluated by means of spectrophotometric detection at 420 nm (Lamba 25, Perkin-Elmer, I). The nanoparticles produce an opalescent colloidal suspension. The turbidity of the colloidal suspension increases up to a maximum following the addition of the cross-linking agent (TPP): according to the literature this maximum corresponds to

the amount of TPP necessary to obtain the maximum yield in nanoparticles. Any further addition of TPP produces nanoparticle aggregation: these aggregates (particle suspension) precipitate causing a decrease in turbidity. On the basis of these results, nanoparticles were prepared using the amount of TPP necessary to obtain the maximum yield without particle aggregation: in the case of CS·HCl and TMC3 a final nanoparticle concentration of 0.28 mg/ml of TPP was used, while in TMC1 and TMC2 nanoparticles were prepared using 0.42 mg/ml of TPP.

The nanoparticles were spontaneously formed upon the incorporation of TPP to the polymer solution under vigorous stirring. The FD4 loaded nanoparticles were prepared using the same procedure: FD4 was dissolved at 10 mg/ml in TPP solution obtaining the final concentration ranging from 0.22 (for CS·HCl and TMC3 nanoparticles) to 0.33 mg/ml (TMC1 and TMC2 nanoparticles) in the polymer–TPP mixture, depending on the polymer–TPP ratio used.

Nanoparticles were centrifuged at 10,000*g* for 30 min and suspended at the desired concentration (3.5 mg/ml) for characterization and the in vitro and ex vivo investigations in Hanks' balanced salt solution (HBSS: $CaCl_2$ anhydrous 140 mg/l, $MgCl_2{\cdot}6H_2O$ 100 mg/l, $MgSO_4{\cdot}7H_2O$ 100 mg/l, KCl 400 mg/l, KH_2PO_4 60 mg/l, $NaHCO_3$ 350 mg/l, NaCl 8000 mg/l, Na_2HPO_4 48 mg/l, D-glucose 1000 mg/l, Phenol Red 10 mg/l, Gibco-BRL, NY, USA) buffered at pH 5.5 with HCl 1 N.

2.2.2. Nanoparticle characterization

The size distribution and the mean particle size were determined by means of a Coulter Counter method. The Coulter Counter apparatus (Coulter Multisizer II, Beckman Coulter, UK) was equipped with a 15 μm orifice diameter tube (size range: 0.427–13.30 μm). Each nanoparticle suspension was diluted in prefiltered physiologic solution (0.9% w/v NaCl) following the procedure of the apparatus. Each sample was dispersed by means of an ultrasound apparatus (Julabo USR8, Julabo Labortechnik GmbH, G) for 5 min to disaggregate the nanoparticles and three subsequent measurements were performed for each sample. The data were recorded and processed by means of software (Coulter Multisizer, AccuComp, ver. 3.01a, Beckman Coulter, UK). In order to validate the Coulter Counter measurements, CLSM microphotographs of each sample were taken.

The manufacturing yield of each nanoparticulate system was calculated following the procedure described below. Each nanoparticle suspension was centrifuged as previously described, and the supernatant removed. The precipitated nanoparticles were rinsed twice with distilled water, and freeze dried (Powerdry LL 1500–55, Heto, Analitica De Mori, I). The yield % was calculated as the ratio between the freeze dried sample weight and the expected weight.

The percent value of FD4 loaded (FD4 % loaded) was calculated as follows: first the amount of drug associated with nanoparticles was calculated as the difference between the total amount of FD4 added to the system called $FD4_t$ (theoretic) and FD4 recovered in the supernatant assuming that the FD4 not recovered in the supernatant was encapsulated in the nanoparticles. Subsequently the ratio between FD4 encapsulated in nanoparticles and the nanoparticles amount (yield) was calculated and expressed as percentage (% FD4 loaded): according to the following equation:

$$\text{FD4 loaded } \% = (FD4_t - FD4_s)/NP * 100$$

where $FD4_t$ is the FD4 theoretic amount employed for nanoparticle preparation, $FD4_s$ is the FD4 free amount recovered in the supernatant, NP is the amount of nanoparticles prepared as calculated by the manufacturing yield.

FD4 remaining in the supernatant or loaded into the nanosystems was assayed by means of a spectrofluorimeter (LS50B, Perkin-Elmer, I) at $\lambda_{ex} = 485$ nm and $\lambda_{em} = 515$ nm.

The encapsulation efficiency (EE%) of FD4 was calculated as the ratio between FD4 loaded into the nanoparticulate systems with respect to the total amount of FD4 employed for nanoparticle preparation as follows [26]:

$$EE\ \% = (FD4_t - FD4_s)/FD4_t * 100$$

where $FD4_t$ is the FD4 theoretic amount employed for nanoparticle preparation, $FD4_s$ is the FD4 free amount recovered in the supernatant.

2.2.3. Permeability studies performed by means of Caco-2 cell monolayer

The nanoparticle suspensions prepared in pH 5.5 HBSS were subjected to permeability tests across Caco-2 cell monolayers.

Caco-2 cells (TC7) (passage 37) were seeded on tissue-culture-treated polycarbonate filters (area 113.1 mm^2; inner diameter 13.85 mm) in 12-well plates (Greiner Bio-one, PBIinternational, Italy) at seeding density of 2.5×10^5 cells/cm^2. Dulbecco's modified Eagle's medium (DMEM, pH 7.40; Bioindustries, Israel) supplemented with 10% foetal bovine serum, benzylpenicillin G (160 U/ml) and streptomycin sulphate (100 μg/ml) (Bioindustries, Israel) and also with 1% nonessential aminoacids (Sigma, I) was used as culture medium. Cell cultures were kept at 37 °C in an atmosphere of 95% air and 5% CO_2 and 95% of relative humidity. Filters were used for transepithelial electrical resistance (TEER) measurements and transport experiments 21–23 days after seeding.

Five hundred microliters of the nanoparticle suspensions at 3.5 mg/ml in HBSS at pH 5.5, prepared as previously described in the "Nanoparticle preparation" paragraph, were used as the apical (donor) phase of the monolayers. HBSS at pH 7.4 (2 ml) was used as the basolateral (receptor) phase and added to the basolateral side of the monolayers. At 0.5, 1, 2, 3 h each filter and its mounting donor chamber filled at the apical phase was moved into a fresh basolateral (receptor) phase. All the receptor phases were collected and the permeated FD4 was assayed

by means of the spectrofluorimetric method previously described. After 3 h, the apical and the basolateral phases were withdrawn and each Caco-2 monolayer was rinsed and put in contact with a LY solution at 25 μg/ml in HBSS and fresh HBSS as basolateral phase. After 1 h contact time the permeated LY was assayed by means of a spectrofluorimetric method ($\lambda_{ex} = 428$ nm; $\lambda_{em} = 521$ nm). The apparent permeability coefficient (P_{app}) was calculated using the following equation [19]:

$$P_{app} = dQ/dt/(A \cdot 60 \cdot C_0)$$

where dQ/dt is the permeability rate (drug amount permeated per min), A is the diffusion area of the monolayer, C_0 is the initial FD4 or LY concentration.

The FD4 recovery was subsequently calculated according to the following equation:

$$\%\ \text{FD4 recovery} = (FD4^{t3}_{apical} + FD4^{t3}_{basolateral})/FD4^{t0}_{apical} * 100$$

where $FD4^{t3}_{apical}$ is the amount of FD4 remained in the apical phase at the end of the permeation experiment (3 h), $FD4^{t3}_{basolateral}$ is the amount of FD4 recovered in the basolateral phase at the end of the permeation experiment (3 h), $FD4^{t0}_{apical}$ is the amount of FD4 present in the apical phase at the beginning of the permeation experiment (3 h).

During the experiments the integrity of the monolayers was assessed by means of TEER measurements at fixed times using a Millicell ERS-meter (Millipore Corp., Bedford, MA, USA).

Twenty-four hours after the end of the permeation experiment, each filter supporting the monolayers was mounted onto microscope slides for the observation at CLSM.

2.3. Mucoadhesion measurements

A Franz diffusion cell (Permeager, USA) with a donor chamber modified as described in [27,28] was used. Briefly, in the donor chamber, a stream of buffer was maintained through two holes. The incoming buffer flux was regulated by means of an HPLC pump (model 300, Gynkotek, Munich, G). The outcoming buffer was collected in a beaker and continuously stirred. Rat jejunum tissue was placed between the donor and acceptor chambers of the cell laying on a filter paper disc imbibed in HBSS in turn placed on a Parafilm® membrane (impermeable to fluids). The receptor chamber of the cell was filled with distilled water whose only function was to keep the jejunum tissue thermo-regulated. The nanoparticulate suspension (500 μl) was placed on the excised rat jejunum (area = 2 cm^2) and physiologic solution (NaCl 0.9% w/v) at 37 °C was fluxed at 0.7 ml/min over the formulation to mimic the washing action of intestine fluids. Five hundred microlitre samples of the fluid outcoming from the donor chamber were withdrawn at fixed times. The amount of drug "washed away" was determined in a receptor beaker at defined times by means of a spectrofluorimetric method.

The amount of nanoparticles not removed by the buffer stream adhered and interacted with the biological substrate providing an indirect evaluation of the mucoadhesion.

2.4. Permeation measurements across excised rat jejunum tissue

The nanoparticles, suspended in HBSS buffered at pH 5.5, were subjected to permeation measurement by means of Franz diffusion cells with a 2 cm^2 orifice area (Permeagear, USA) thermostated at 37 °C. Freshly excised rat jejunum tissue, laying on a filter paper, was placed between the donor and the acceptor chambers of the Franz diffusion cell. Each nanoparticle suspension (500 μl) was placed in the donor chamber on rat jejunum tissue. HBSS (pH 7.4) was used as acceptor phase (sink conditions in the acceptor phase were maintained during the test).

At fixed time intervals, 500 μl samples of the acceptor phase were withdrawn and replaced with fresh buffer. FD4 was assayed by means of spectrofluorimetric detection.

The permeation test was also performed by using FD4 solution in HBSS, pH 5.5, having the same concentration of nanoparticulate systems.

The apparent permeability coefficient (P_{app}) was calculated using the equation [18] previously described.

2.5. Evaluation of nanoparticle penetration into excised rat jejunum tissue

The nanoparticle suspensions in HBSS, pH 5.5, were subjected to penetration measurements in excised rat jejunum tissue by means of a Franz diffusion cell. The rat jejunum was employed immediately after the death of the animals. Each nanoparticle suspension (500 μl) was applied on rat jejunum tissue (area = 2 cm^2) fixed between the donor and the receptor chamber of a Franz diffusion cell. The acceptor chamber was filled with pH 7.4 HBSS to maintain the mucosa hydrated and thermostated.

The penetration test was also performed by using FD4 solution in HBSS, pH 5.5, having the same concentration as the nanoparticulate systems.

At the end of the experiment (1 h) the sample was removed from the tissue which was rinsed twice with pH 7.4 HBSS, was included in the OTC compound (Leika Microsystem, G), frozen in liquid nitrogen and stored at −80 °C.

2.6. Statistical evaluation

Statistical differences were determined using one-way ANOVA and post hoc Sheffe tests for multiple comparisons (Siphar, Creteil, F). Differences between groups were considered to be significant at $p < 0.05$.

2.7. Confocal laser scanning microscopy (CLSM)

CLSM was utilized to visualize the eventual internalisation of nanoparticles. 24 h after the end of the permeation experiments performed in vitro with Caco-2 cell monolayer, the filter, with the cell monolayer, was dehydrated for 12 h and subsequently fixed by dipping in ethanol. Each filter was placed on a microscope slide.

For the observation of tissue samples, slices perpendicular to the mucosa surface, 10 μm in thickness, were cut from the rat jejunum included in the OTC Compound using a cryostat (Leica CM1510, Leica Microsystem, I) at −20 °C. Each slice was placed on a microscope slide, dehydrated for 12 h and subsequently fixed by dipping the microscope slides in acetone.

The nuclei of cell monolayers and of the tissue slice were stained by dipping the biological substrates into a solution (1:100,000) of Hoechst 33258 (Sigma, I).

Each microscope slide, either with Caco-2 cell monolayer on a filter or with a rat jejunum slice, was mounted using PVA-DABCO, polyvinyl alcohol mounting medium with DABCO antifading (mixture of tris(hydroxymethyl)aminomethane, tris/hydroxymethyl)aminomethane hydrochloride, polyvinyl alchol 22,000 Da, glycerol anhydrous and 1,4-diazabicyclo[2,2,2]octane; (BioChemika, Fluka, I) and covered with cover glass.

The slides were observed using a Confocal Laser Scanning Microscope using $\lambda_{ex} = 485$ nm and $\lambda_{em} = 515$ nm for the visualization of FD4 and $\lambda_{ex} = 346$ nm $\lambda_{em} = 460$ nm for the visualization of Hoechst 33258. The acquired images were processed by means of a software (Leika Microsystem, I).

To obtain depth information from specific sections (*xz*- and *yz*-sections), the confocal images of *xy* planes were first acquired (parallel to the plane of the slice surface). To generate the *xz*- and the *yz*-sections, two horizontal lines were drawn across the regions of interest in the $z = 0$ μm-*xy*-plane, and the digitalized image data of the successive *xy*-sections were optically sliced through along the *z*-axis. The result was the *xz*- and *yz*-planar optical cross-sections [29].

3. Results and discussion

3.1. Nanoparticle characterizations

Table 1 shows diameters (nm) and preparation yields (%) of all the nanoparticulate systems, blank and FD4 loaded. In the case of the FD4 loaded nanoparticulate systems, the FD4 loading (%) and the encapsulation efficiency (EE%) are also given.

The loading of FD4 into all the nanoparticulate systems did not cause any significant differences in particle size: this result demonstrated that the FD4 association in the nanoparticulate systems did not produce an increase in particle size. Furthermore, for all the nanoparticulate systems, the chitosan amino group quaternization, through trimethylation, corresponded to a decrease in particle size; this effect becomes more evident with the increase in the quaternization degree (QD) of the trimethylchitosan (TMC) ($p < 0.01$). Fig. 1 shows a CLSM microphotograph of TMC1 (lower quaternization degree) nanoparticles as an example. The nanoparticles are characterized by a spherical shape.

As for the production yields of the blank systems, nanoparticles based on TMC3 presented the lowest yield percentage (about 6%) ($p < 0.05$) followed by CS·HCl (10%) ($p < 0.05$), TMC2 (19%) ($p < 0.001$) and TMC1 (64%) ($p < 0.001$). In the case of FD4 loaded systems, nanoparticles based on CS·HCl (the starting chitosan) showed the lowest production yield (10%) ($p < 0.05$) while the systems based on TMC1 (having the lowest QD) and TMC2 (having the intermediate QD) were characterized by similar yields (about 25–30%). The systems based on TMC3 (having the highest QD) showed slightly, but significantly, lower production yield (20%) with respect to the other trimethylchitosan systems ($p < 0.05$). Only for the system based on CS·HCl, the FD4 loading did not change the production yield.

Nanosystems based on CS·HCl and TMC3 showed comparable percentages of the FD4 loaded even if CS·HCl nanoparticles presented a slightly higher FD4 association

Table 1
Particle size (nm), yield of preparation (%), FD4 loaded (%), encapsulation efficiency (EE) (%) evaluated for all the nanoparticulate systems with and without FD4 (mean values ± SD; $n = 6$)

		Particle size (nm)	Yield %	FD4 loaded %	EE%
CS·HCl	Blank	904 ± 77	8.57 ± 4.04		
	FD4	1034 ± 48	10.84 ± 0.83	89.82 ± 0.88	89.82 ± 0.87
TMC1	Blank	862 ± 78	64.01 ± 0.01		
	FD4	1015 ± 68	25.29 ± 3.25	47.92 ± 0.24	87.86 ± 0.44
TMC2	Blank	808 ± 4	18.67 ± 3.77		
	FD4	779 ± 19	34.48 ± 9.75	35.10 ± 0.02	87.75 ± 0.07
TMC3	Blank	577 ± 6	5.71 ± 0.01		
	FD4	588 ± 0.82	17.95 ± 3.63	86.94 ± 0.08	86.94 ± 0.09

CS·HCl, starting chitosan.
TMC1, quaternization degree of 4%.
TMC2, quaternization degree of 35%.
TMC3, quaternization degree of 90%.
EE, encapsulation efficiency.

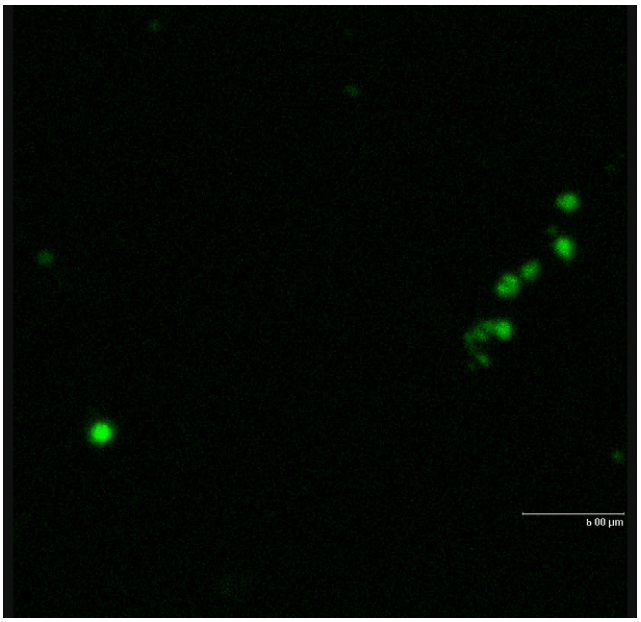

Fig. 1. CLSM microphotograph of TMC1 nanoparticles (as example).

($p < 0.001$). In the other nanoparticulate systems the percentages of FD4 loaded were lower: in particular, TMC2 showed the lowest FD4 loading percentage with respect to all of the other systems ($p < 0.001$). Since all the nanoparticulate systems showed only slightly different encapsulation efficiency values (EE%) (CS·HCl > TMC1 ≅ TMC2 > TMC3; $p < 0.05$) the FD4 loading percentages strictly depended on the production yields. The nanosystems based on CS·HCl and TMC3 are characterized by FD4 % loaded of about 90%. This is probably due to the amount of TPP used to prepare the systems which was lower than that used for TMC1 and TMC2 preparations, as the aggregation of particles due to the additions of higher amounts of TPP did not allow the employment of preparation conditions of the other nanosystems.

3.2. Permeability studies performed by means of Caco-2 cell monolayer

Fig. 2 reports the Papp (cm/s) values of FD4 (the model macromolecule) and Lucifer Yellow (LY) (the fluorescent probe which is not permeable in the presence of intact tight junctions) calculated for all of the nanoparticulate systems and for the FD4 solution tested as Control.

The nanoparticulate systems based on CS·HCl, TMC1 and TMC2 were characterized by Papp values for FD4 significantly higher than that of Control ($p < 0.01$). Moreover, they were also characterized by comparable Papp values (not significantly different). On the contrary, the nanosystem of TMC3 showed FD4 Papp value not significantly different from that of the Control: this indicates that the transport of FD4 across the Caco-2 cell monolayer was not improved by the presence of the TMC3 nanoparticles.

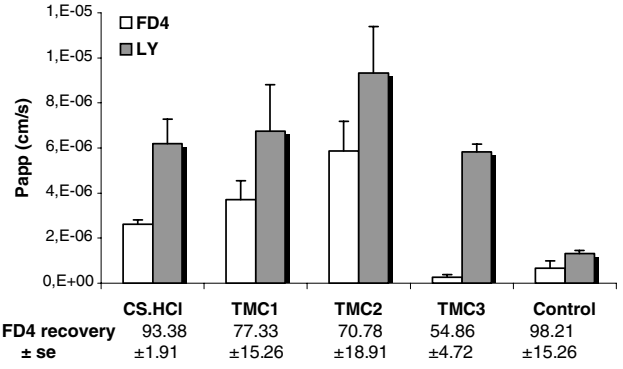

	CS.HCl	TMC1	TMC2	TMC3	Control
% FD4 recovery	93.38	77.33	70.78	54.86	98.21
± se	±1.91	±15.26	±18.91	±4.72	±15.26

Fig. 2. Papp (cm/s) values of FD4 and LY calculated for permeability experiment performed using Caco-2 cell monolayers observed for all the nanoparticulate systems and the Control, FD4 solution (mean values ± SE; $n = 6$). In the inset the FD4 amount % recovery that followed permeability experiment are reported (mean values ± SE; $n = 6$).

Looking at the total amounts of FD4 recovered and reported in the inset below Fig. 2, it is possible to see that the nanosystem based on TMC3 was characterized by the lowest percentage of FD4 amount recovered (about 55%) ($p < 0.05$). All the other nanoparticulate systems presented variable recovery percentages, even though in no cases could a statistically significant difference be appreciated with respect to the FD4 solution (Control). One of the hypotheses that could explain the low recovery of FD4 following the treatment of Caco-2 monolayers with nanoparticles based on TMC3 is that in this sample the FD4 loaded nanoparticles are entrapped in the cells.

The Papp values of Lucifer Yellow, the fluorescent marker of the paracellular pathway, calculated for the Caco-2 monolayer treated with all the nanoparticulate systems were significantly higher than that of the monolayer treated only with the FD4 solution. This indicates that for all of the samples, the contact with the nanoparticulate systems produced an opening of the junction complexes (tight junctions) between the cells.

These results were also confirmed by the TEER % profiles (Fig. 3). All the nanoparticulate systems showed TEER % profiles significantly lower than that of the

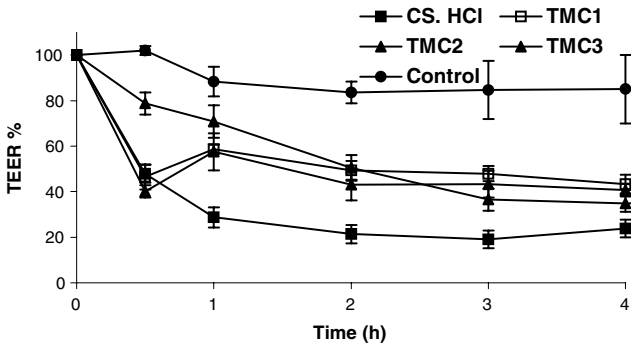

Fig. 3. TEER % vs time profiles observed for all the nanoparticulate systems and the Control, FD4 solution (mean values ± SE; $n = 6$).

Control ($p < 0.05$) and all comparable to each other. In the first time (at 30 min) of the TEER profile, the nanoparticulate system based on TMC3 presented a slower decrease of the TEER % in comparison with all the other nanoparticles ($p < 0.05$) to indicate a slower induction of the interactions with the biological substrate. The lowering of the transepithelial electrical resistance % (TEER %) profiles implicates that all the nanoparticulate systems, excluding the difference previously mentioned, were responsible for the modulation of the cell junction integrity: this feature was also supported by the permeation of the LY across the cell monolayers treated with the nanoparticles. These results are in agreement with those previously reported by Ma and Lim [5].

Fig. 4 reports the CLSM microphotographs of the Caco-2 monolayers treated with the nanosystems [(a) CS·HCl; (b) TMC1; (c) TMC2; (d) TMC3] and the confocal *xz*-image microphotograph of the TMC2 sample, given as an example.

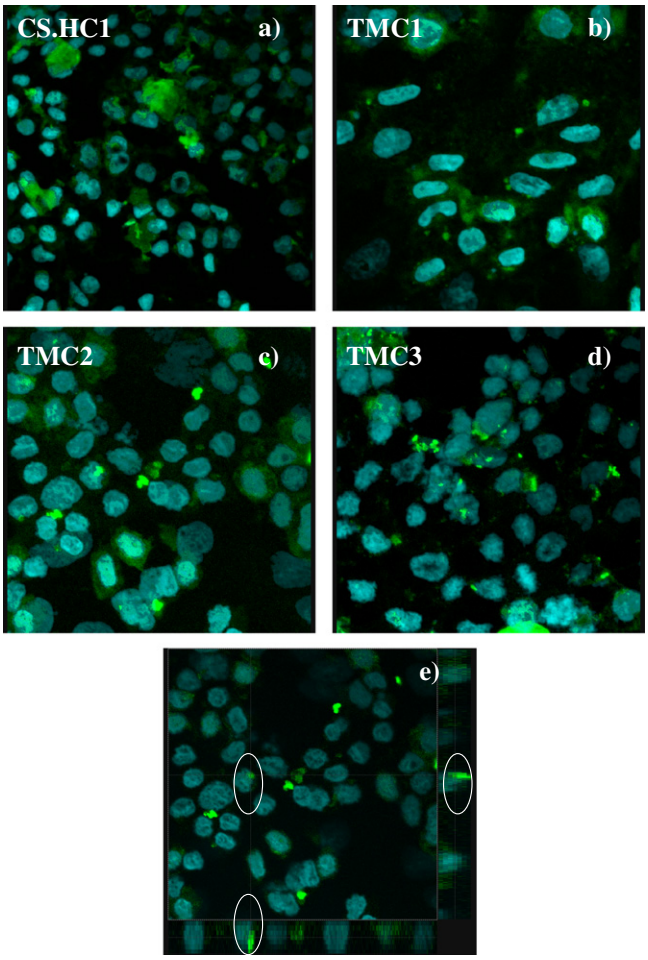

Fig. 4. CLSM microphotograph of the Caco-2 monolayers with nanoparticles obtained after the permeation experiment: (a) CS·HCl; (b) TMC1; (c) TMC2; (d) TMC3; (e) CLSM microphotograph with *xz*- and *yz*-sections of a Caco-2 monolayer treated with TMC2 nanoparticles (as an example an encircled nanoparticle in the *xy*-plane and in both the *xz*- and *yz*-sections is shown).

The Caco-2 monolayer treated with the nanoparticles based on CS·HCl presented diffuse green spots of FD4 close to the blue spots of the nuclei to indicate that the model macromolecule was present in the cells but no longer entrapped in the nanosystems (Fig. 4a).

The Caco-2 monolayers after the contact with the nanoparticulate systems based on TMC1 and TMC2 were characterized by the presence, close to the nuclei, of some thick green spots, with the particle size comparable to that of the nanoparticles: this feature indicates that not only the nanopaticulate systems were internalised into the Caco-2 cells but also that they could be found intact up to 24 h in the cells (Figs. 4b and c). The three-dimensional *xz*- and *yz*-projections of a CLSM microphotograph (nanoparticles based on TMC2 as example) demonstrated that the nanoparticles were deeply penetrated into the cells, due to the presence of the nanoparticles close to the nuclei (Fig. 4e).

The Caco-2 cell monolayer after the contact with nanoparticles based on TMC3 showed the presence of an even higher number of thick green spots, localized in the cells close to the nuclei, characterized by sizes comparable to those of the nanoparticles. This is illustrated in Fig. 4d. The major internalization of the TMC3 nanoparticles into the Caco-2 cells could reasonably explain the low value of FD4 Papp (comparable to that of the Control) and also by the low recovery of FD4.

In all the CLSM microphotographs, the staining of Caco-2 cell nuclei highlighted the fact that the chromatin resulted as dense as that of viable cells, indicating the lack of a markedly toxic effect of any of the nanoparticulate systems.

3.3. Mucoadhesion properties

Fig. 5 shows the profiles of FD4 amount % washed away vs time obtained by the different nanoparticulate systems and the Control using the rat jejunum as a biological substrate. All the nanoparticulate systems were characterized by profiles lower than that of the Control up to 45 min ($p < 0.05$) while, due to measurement variability, there were no significant differences between the nanopar-

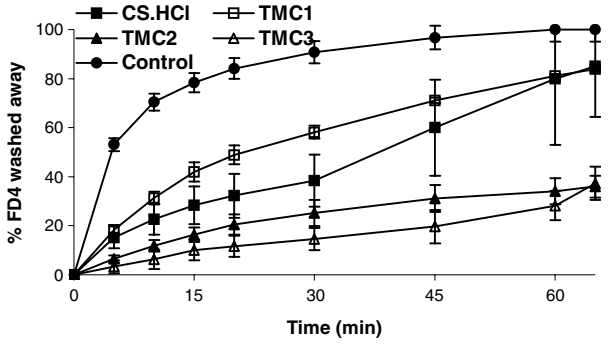

Fig. 5. FD4 amount % washed away vs time profiles observed for all the nanoparticulate systems and the Control, FD4 solution (mean values ± SE; $n = 6$).

ticulate systems up to 45 min. For longer times, the systems based on TMC2 and TMC3 were characterized by lower washed away profiles ($p < 0.05$). In the experiment and in the tissue preparation before the experiment, care was taken in order to maintain the mucus layer that covered the tissue, and moreover, the freshly excised jejunum tissue was still mucus secreting during the experiment. The results show that the nanoparticles were able to strongly adhere to the mucus layer significantly prolonging their in vivo residence on mucosa surface, with respect to the Control.

Even if all the nanoparticulate systems were able to interact with the biological substrate, the increase in quaterization degree of trimethylchitosan seems to confer a greater resistance toward the removal effect of the buffer stream, as can be seen for the samples TMC2 and TMC3, which resisted the washing action up to 1 h.

3.4. Permeation measurements across excised rat jejunum tissue

Fig. 6 shows Papp (cm/s) values of FD4 calculated from permeability experiments performed using excised rat jejunum with all the nanoparticulate systems and the FD4 solution (Control).

All the nanosystems showed Papp values markedly higher than that of the Control ($p < 0.001$). Nanoparticles based on TMC1 and TMC2 were characterized by the highest Papp values, and not significantly different from each other ($p < 0.01$) while the nanoparticulate systems based on CS·HCl and TMC3 presented similar Papp values. The effect of chitosan trimethylation on the FD4 permeation is characterized by an increase up to an optimal value corresponding to the intermediate degree (TMC2), the FD4 permeation dropped at the maximum quaternization degree. In this regard, the ex vivo trend exactly reflects the in vitro one.

3.5. Evaluation of nanoparticle penetration into excised rat jejunum tissue

An insight into the possible reasons for the permeation trends was found in the CLSM observation of the tissue samples after 1 h and after 3 h of treatment with nanoparticle samples.

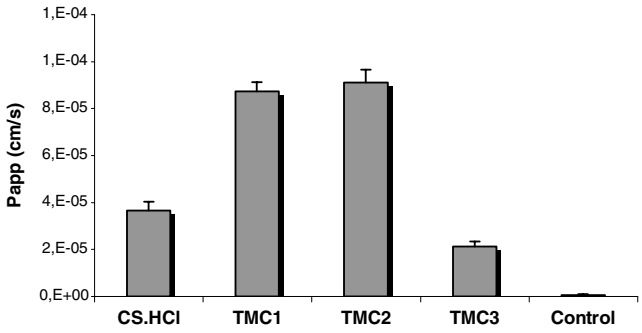

Fig. 6. Papp (cm/s) values of FD4 calculated for permeability experiment performed using excised rat jejunum observed for all the nanoparticulate systems and the Control, FD4 solution (mean values ± SE; $n = 6$).

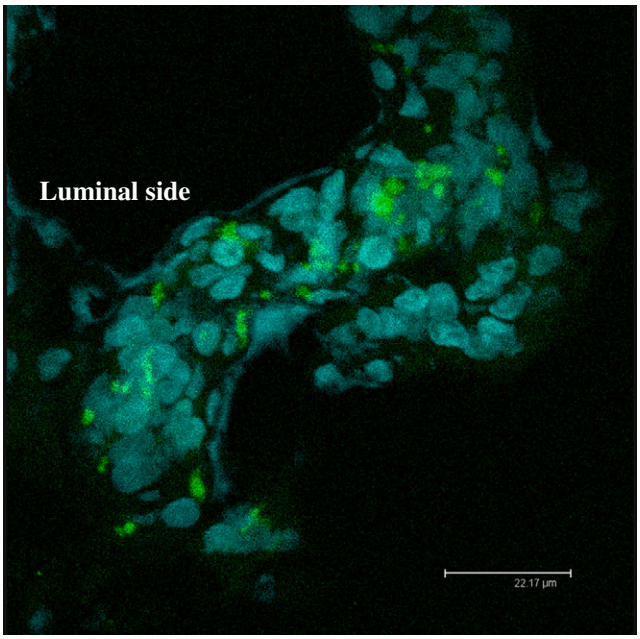

Fig. 7. CLSM microphotograph of the cross section (10 µm) of rat jejunum treated with TMC1 nanoparticles obtained after the penetration experiment (1 h of contact time).

Fig. 7 shows the CLSM of rat jejunum after the contact with TMC1 nanoparticles.

After 1 h of contact time the nanoparticles based on both CS·HCl and TMC1 were located inside the tissue close to the cell nuclei: this result evidenced the capability of these nanoparticulate systems to penetrate into the tissues.

Fig. 8 shows the CLSM of rat jejunum after the contact with TMC2 nanoparticles as an example. In this case, as for the TMC3 (data not shown) after 1 h of contact time the nanoparticles were located on the rat jejunum surfaces conceivably as a consequence of the strong mucoadhesive joint between the nanoparticles and the mucus layer covering the epithelial cells: this behaviour was in line with the washability experiment, in which TMC2 and TMC3 nanosystems showed the lowest wash away profiles. The mucoadhesive properties could slow down the absorption of nanoparticles into the cells with a sort of sequestering effect. In spite of this effect that could be an obstacle for nanoparticle absorption, the prolongation of the residence time offered more possibilities of nanoparticle internalisation.

Fig. 9 shows a CLSM microphotograph of the rat jejunum after the contact with TMC3 nanoparticles as an example. After 3 h of contact time, green spots (that can be identified with FD4 loaded nanoparticles) could be found in the intestinal tissue in contact with the cell nuclei, for all the nanoparticulate systems, confirming that all of them were able to interact with the jejunum tissue and be internalised in it.

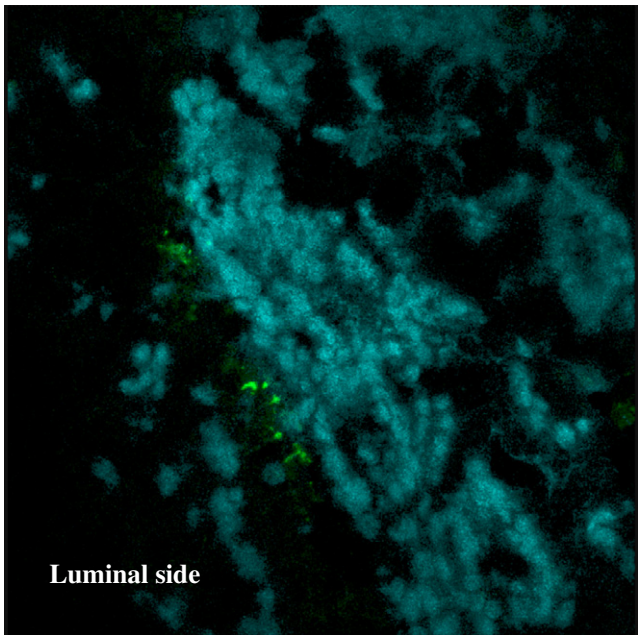

Fig. 8. CLSM microphotograph of the cross section (10 μm) of rat jejunum treated with TMC2 nanoparticles obtained after the penetration experiment (1 h of contact time).

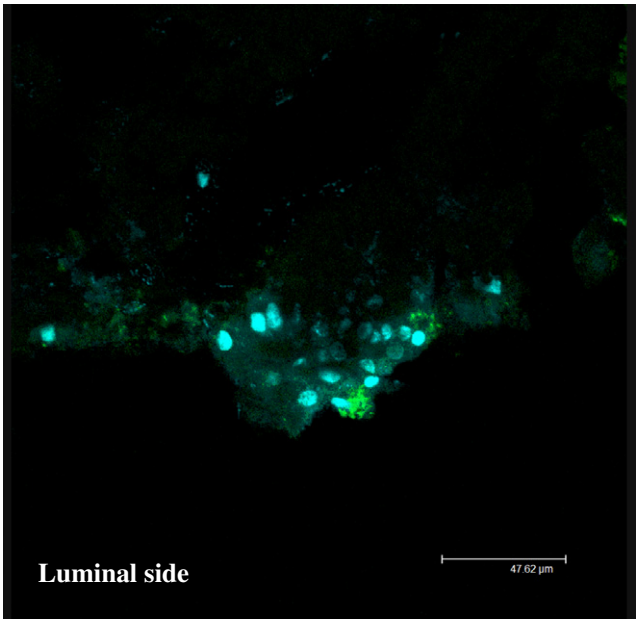

Fig. 9. CLSM microphotograph of the cross section (10 μm) of rat jejunum after the contact with TMC2 nanoparticles (as example) obtained after the permeation experiment (3 h of contact time).

4. Conclusions

The ionotropic gelation method was suitable to prepare nanoparticles based on trimethylchitosans with good encapsulation efficiency of fluorescein isothiocyanate dextran, the model macromolecule having molecular weight comparable to that of proteins commonly employed in therapy (such as insulin 5733 Da and calcitonin 3417 Da).

The "in vitro" approach evidences that all the nanoparticulate systems increased the widening of the paracellular pathway. The nanosystems based on CS·HCl, TMC1 and TMC2 were able to improve the permeability of FD4. On the contrary, the TMC3 nanosystem, in spite of its capability to enlarge the paracellular pathway, did not increase FD4 permeability with respect to the FD4 solution (Control): this is probably due the long lasting entrapment of nanoparticles into Caco-2 cells (evidenced by a large amount of green spots corresponding to nanoparticles visible in the CLSM microphotograph).

The "ex vivo" approach, to evaluate penetration enhancement properties, confirms the same trend of the "in vitro" one (Caco-2 cells). The increase in quaternization degree of trimethylchitosan favours the mucoadhesion, conceivably resulting in a prolonged residence time of the nanosystems and consequently in a greater chance of internalisation.

The comparison of mucoadhesive and penetration enhancement properties points out that the mucoadhesive properties slow down the absorption of nanoparticles through the mucus layer into the cell. However, the increase of the contact between the intestinal epithelium and the nanosystems should offer more possibilities for nanoparticle internalisation.

The improvement of mucoadhesion and of nanoparticle internalisation capabilities makes trimethylchitosan-based nanosystems suitable carriers for the oral administration of macromolecules and, in particular, of peptides.

Acknowledgement

This study was supported by funding from the Italian Ministry of University and Scientific Research (MIUR) (PRIN/COFIN 2005).

References

[1] A.T. Florence, A.M. Hillery, N. Hussain, P.U. Jani, Nanoparticles as carriers for oral peptide absorption: studies on particle uptake and fate, J. Control. Rel. 36 (1995) 39–46.
[2] H. Takeuki, H. Yamamoto, Y. Kawashima, Mucoadhesive nanoparticulate systems for peptide drug delivery, Adv. Drug Del. Rev. 47 (2001) 39–54.
[3] K.A. Janes, P. Calvo, M.J. Alonso, Polysaccharide colloidal particles as delivery systems for macromolcules, Adv. Drug Del. Rev. 47 (2001) 57–83.
[4] G. Ponchel, M.-J. Montisci, A. Dembri, C. Durrer, D. Duchene, Mucoadhesion of colloidal particulate systems in the gastrointestinal tract, Eur. J. Pharm. Biopharm. 44 (1997) 25–31.
[5] Z. Ma, L.-Y. Lim, Uptake of chitosan associated insulin in Caco-2 cell monolayers: a comparison between chitosan molecules and chitosan nanoparticles, Pharm. Res. 20 (11) (2003) 1812–1819.
[6] C.M. Lehr, J.A. Bouwstra, E.H. Schacht, H.E. Junginger, In vitro evaluation of mucoadhesive properties of chitosan and some other natural polymers, Int. J. Pharm. 78 (1992) 43–48.

[7] I. Henriksen, K.L. Green, J.D. Smart, G. Smistad, J. Karlsen, Bioadhesion of hydrated chitosans: an in vitro and in vivo study, Int. J. Pharm. 145 (1996) 231–240.
[8] P. Artursson, T. Lindmark, S.S. Davis, L. Illum, Effect of chitosan on the permeability of monolayers of intestinal epithelial cells (Caco-2), Pharm. Res. 11 (1994) 1358–1361.
[9] V. Dodane, A. Amin Khan, J.R. Mervin, Effect of chitosan on epithelial permeability and structure, Int. J. Pharm. 182 (1999) 21–32.
[10] M. Huang, E. Khor, L.Y. Lim, Uptake and citotoxicity of chitosan molecules and nanoparticles: effects of molecular weight and degree of deacetylation, Pharm. Res. 21 (2004) 344–353.
[11] R. Fernandez-Urrursuno, P. Calvo, C. Remunan-Lopez, J.L. Vila-Jato, M.J. Alonso, Enhancement of nasal absorption of insulin using chitosan nanoparticles, Pharm. Res. 16 (1999) 1576–1581.
[12] A.M. Dryer, M. Hinchcliffe, P. Watts, J. Castile, I. Jabbal-Gill, R. Nankervis, A. Smith, L. Illum, Nasal delivery of insulin using novel chitosan formulations: a comparative study in two animal models between simple chitosan formulations and chitosan nanoparticles, Pharm. Res. 19 (2002) 998–1008.
[13] A.M. De Campos, A. Sanchez, M.J. Alonso, Chitosan nanoparticles: a new vehicle for the improvement of the delivery of drugs to the ocular surface. Application to cyclosporin A, Int. J. Pharm. 224 (2001) 159–168.
[14] I. Behrens, A.I. Vila-Pena, M.-J. Alonso, T. Kissel, Comparative uptake studies of bioadhesive and non-bioadhesive nanoparticles in human intestinal cell lines and rats: the effect of mucus on particle absorption and transport, Pharm. Res. 19 (2002) 1185–1193.
[15] M. Huang, E. Khor, L.Y. Lim, Uptake and citotoxicity of chitosan molecules and nanoparticles: effects of molecular weight and degree of deacetylation, Pharm. Res. 21 (2004) 344–353.
[16] M.M. Thanou, A.F. Kotzé, T. Scharringhausen, H.L. Lueßen, A.G. de Boer, J.C. Verhoef, H.E. Junginger, Effect of degree of quaternization of *N*-trimethyl chitosan chloride for enhanced transport of hydrophilic compounds across intestinal Caco-2 cell monolayers, J. Control. Rel. 64 (2000) 15–25.
[17] A.F. Kotzé, H.L. Lueßen, B.J. de Leeuw, A.G. de Boer, J.C. Verhoef, H.E. Junginger, *N*-trimethyl chitosan chloride as a potential absorption enhancer across mucosal surface: in vitro evaluation in intestinal epithelial cells (Caco-2), Pharm. Res. 14 (1997) 1197–1202.
[18] A.F. Kotzé, H.L. Lueßen, B.J. de Leeuw, A.G. de Boer, J.C. Verhoef, H.E. Junginger, Comparison of the effect of different chitosan salts and *N*-trimethyl chitosan chloride on permeability of intestinal epithelial cells (Caco-2), J. Control. Rel. 51 (1998) 35–46.
[19] C. Jonker, J.H. Hamman, A.F. Kotzè, Intestinal paracellular permeation enhancement with quaternized chitosan: in situ and in vitro evaluation, Int. J. Pharm. 238 (2002) 205–213.
[20] P. Sinswat, P. Tengamnuay, Enhancing effect of chitosan on nasal absorption of salmon calcitonin in rats: comparison with hydroxypropyl- and dimethyl-β-cyclodextrins, Int. J. Pharm. 257 (2003) 15–22.
[21] A.F. Kotzé, M.M. Thanou, H.L. Lueßen, A.G. de Boer, J.C. Verhoef, H.E. Junginger, Enhancement of paracellular drug transport with highly quaternized *N*-trimethyl chitosan chloride in neutral environments: in vitro evaluation in intestinal epithelial cells (Caco-2), J. Pharm. Sci. 88 (1999) 253–257.
[22] A.B. Sieval, M. Thanou, A.F. Kotzè, J.C. Verhoef, J. Brussee, H.E. Junginger, Preparation and NMR characterization of highly substituted *N*-trimethyl chitosan chloride, Carbohydr. Res. 36 (1998) 165–175.
[23] G. Di Colo, S. Burgalassi, Y. Zambito, D. Monti, P. Chetoni, Effects of different *N*-trimethyl chitosans on in vitro/in vivo ofloxacin transcorneal permeation, J. Pharm. Sci. 93 (2004) 2851–2862.
[24] P. Calvo, C. Remunan-Lopez, J.L. Vila-Jato, M.J. Alonso, Novel hydrophilic chitosan-polyethylene oxide nanoparticles as protein carriers, J. Appl. Polym. Sci. 63 (1997) 125–132.
[25] S. Rossi, F. Ferrari, M.C. Bonferoni, C. Caramella, Characterization of chitosan hydrocloride-mucin interaction by means of viscosimetric and turbidimetric measurements, Eur. J. Pharm. Sci. 12 (2000) 251–257.
[26] K.A. Janes, M.P. Fresneau, A. Marazuela, A. Fabra, M.J. Alonso, Chitosan nanoparticles as delivery systems for doxorubicin, J. Control. Rel. 73 (2001) 255–267.
[27] M.C. Bonferoni, S. Rossi, F. Ferrari, C. Caramella, A modified cell for simultaneous assessment of drug release and washability of mucoadhesive gels, Pharm. Dev. Technol. 4 (1999) 45–53.
[28] S. Rossi, M.C. Bonferoni, F. Ferrari, C. Caramella, Drug release and washability of mucoadhesive gels based on sodium carboxymethylcellulose and polyacrylic acid, Pharm. Dev. Technol. 4 (1999) 55–63.
[29] R. Alvarez-Roman, A. Naik, Y.N. Kalia, H. Fessi, R.H. Guy, Visualization of skin penetration using confocal laser scanning microscopy, Eur. J. Pharm. Biopharm. 58 (2004) 301–316.